# UNDERSTANDING THE BEAM EMITTANCE EVOLUTION DURING STABLE BEAMS BASED ON EMITTANCE SCANS

O. Karacheban* on behalf of the CMS Collaboration
*CERN, Geneva, Switzerland*

*Abstract*

High-luminosity production at the LHC is closely linked to the size of the transverse beam emittance. However emittance measurement is challenging. It is important to use multiple methods for emittance measurement to gain confidence in the absolute value measured and to improve our knowledge of emittance evolution during "stable beams" conditions. In these proceedings, the potential of emittance scans for emittance measurement is studied. Comparison between the emittance measured using emittance scans at CMS in the noncrossing plane and wire scanners is presented. Emittance evolution in the long LHC fills, and comparison to synchrotron light monitors, sources of the systematic uncertainty, and future plans for analyses are described.

## INSTRUMENTS EMPLOYED

Wire Scanners (WS) are the most precise devices used for emittance measurement at LHC, but they cannot be used for all bunches in the machine (limitations are 240 nominal bunches at 450 GeV or 12 bunches at 6.5 TeV) [1].

The Beam Synchrotron Radiation Telescope (BSRT) [2] is the only instrument at LHC continuously measuring emittance bunch by bunch. It is used during the LHC operation for monitoring of the relative change of the emittance during a fill. BSRT cannot be independently calibrated, hence it is cross-calibrated to WS. For the purpose of this calibration, special fills are carried out several times a year at LHC, the so-called "BSRT calibration fills". Several BSRT calibration fills are required, as absolute calibration drifts in BSRT occur due to the radiation damage. A wide range of emittance values from about 1.3 to 5 $\mu$m is covered in these fills, as required for the BSRT calibration. Only nine colliding bunches are injected at nominal LHC beam energy so that WS can perform the emittance measurement for all nine bunches.

CMS online bunch by bunch luminometers [3] have a potential for studying emittance evolution during long LHC fills. Since 2017, emittance scans are regularly performed at the beginning and at the end of each fill [4] at Interaction Point 5 (IP5), where the CMS detector resides. Regular emittance scans and extended emittance scans were also performed in BSRT calibration fills.

## EMITTANCE SCANS IN BSRT CALIBRATION FILLS

In these proceedings, we discuss two BSRT calibration fills, focusing on different aspects. More specifically, fill 6592 from April 2018 was longer and contained emittance scans separated by 2.5 hours in time, as shown in Fig. 1. Therefore, bunch-by-bunch comparison of measurements by CMS in emittance scans and by WS, and emittance evolution are studied based on the first (started at 23:27) and last (started at 01:57) scans, hereafter referred to as emittance scan 1 and emittance scan 6 in the context of fill 6592. Fill 7220 from September 2018 was very short and only contained a regular (9 points) and a long (15 points) emittance scan. In the long scan the effective beam overlap is sampled better. Therefore, more complicated fit models are used to quantify the bias from the fit model selection.

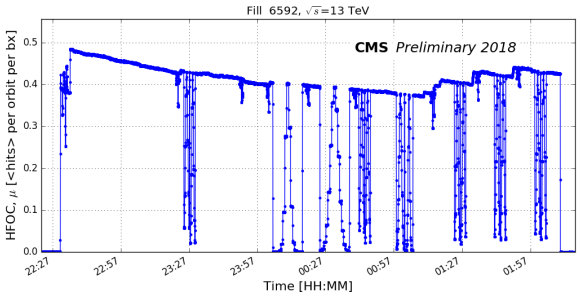


Figure 1: Average number of hits per orbit as measured by the hadron forward calorimeter (occupancy algorithm, HFOC) during stable beams of the BSRT calibration fill 6592. Emittance scans are seen as drops to low (almost to zero) hit values, while LHC optimizations scans are seen as smaller drops before every emittance scan.

As an exmaple, an LHC beam optimisation and emittance scan 1 in the $X$ and $Y$ directions are shown in Fig. 2.

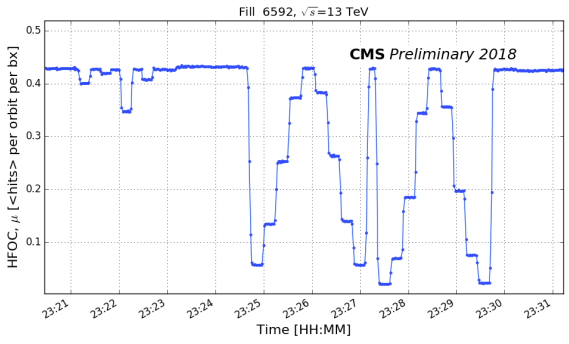


Figure 2: Emittance scan 1 in the BSRT calibration fill 6592: LHC beam optimisation (23:21–23:23), scan in $X$ (23:25–23:27) and scan in $Y$ (23:28–23:30).

* olena.karacheban@cern.ch

### *Effective beam overlap measurement*

The average number of hits per orbit measured during every beam-separation step as a function of the beam separation is used to extract the effective beam overlap in $X$ ($\Sigma_X$) and $Y$ ($\Sigma_Y$) planes. Typically a fit to single Gaussian is used for the emittance scans to measure $\Sigma_{X(Y)}$, as described in detail in Ref. [5]. The effective beam overlap is related to two beam widths as follows:

$$\Sigma^2_{X(Y)} = \sigma^2_{1,X(Y)} + \sigma^2_{2,X(Y)} \tag{1}$$

Multiple CMS luminometers provide $\Sigma_{X(Y)}$ measurements per bunch crossing (BCID). Fig. 3 shows $\Sigma_Y$, measured in emittance scan 1 of fill 6592 by the Hadron Forward (HF) calorimeter (occupancy based algorithm HFOC and transverse energy sum based algorithm HFET), as well as the Fast Beam Condition Monitor (diamond sensors based BCM1F pCVD and silicon sensors based BCM1F Si) [3]. Since nine bunches of different emittance were injected, different effective beam overlaps are measured by CMS luminometers.

The ratio of $\Sigma_Y$ measured by each detectors to HFET $\Sigma_Y$, is shown in Fig. 4. For all bunches the agreement is better than 0.4%, except for the first bunch measured by BCM1F Si. For comparison to WS and further analyses, HFOC and BCM1F pCVD data will be used.

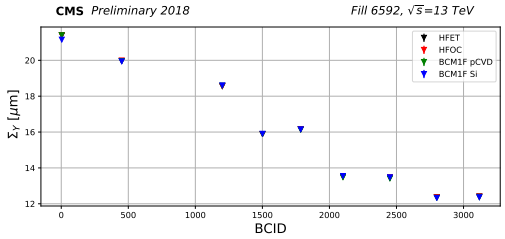


Figure 3: Effective beam overlap $\Sigma_Y$ measured by different luminometers in emittance scan 1 of fill 6592. Single Gaussian fit was used, no corrections are applied.

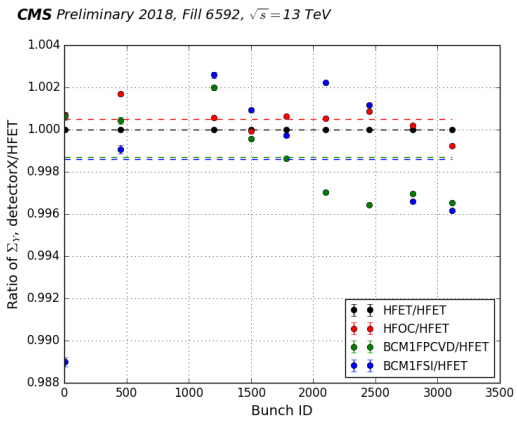


Figure 4: Ratio of $\Sigma_Y$ measured by different luminometers to $\Sigma_Y$ measured by HFET.

### *Recasting beam overlap to emittance*

Assuming $\sigma_{X(Y)} = \sigma_{1,X(Y)} = \sigma_{2,X(Y)}$ and no crossing angle ($\alpha$/2=0), normalized emittance $\varepsilon$ and measured effective beam overlap $\Sigma$ are related by the following equation:

$$\Sigma_{X(Y)} = \sqrt{2}\sigma_{X(Y)} = \sqrt{\frac{2\varepsilon_{X(Y)}\beta^*}{\gamma}} \tag{2}$$

$\beta^*$ is betatron function at the interaction point and $\gamma$ is the relativistic factor defined as ratio of proton beam energy to proton mass $\gamma = 6500$ GeV/0.938GeV. In the presence of a crossing angle (in the $X$ plane for CMS), the calculation includes also longitudinal profile dependency. Assuming Gaussian profile in $Z$, we can calculate $\varepsilon_X$ from measured $\Sigma_X$ as follows:

$$\begin{aligned} \Sigma_X &= \sqrt{\frac{2\varepsilon_X\beta^*}{\gamma}\cos^2(\alpha/2) + 2\sigma_Z^2\sin^2(\alpha/2)}, \\ \varepsilon_X &= \frac{\gamma\Sigma_X^2 - 2\gamma\sigma_Z^2\sin^2(\alpha/2)}{2\beta^*\cos^2(\alpha/2)} \end{aligned} \tag{3}$$

As described in Ref. [4], significant bias to the emittance measured in the crossing plane is expected due to the non-Gaussian profiles of the beam in $Z$ plane. The bias is independently confirmed in the emittance scan analyses performed by LHC colleagues at IP1 (ATLAS), where the crossing plane is in $Y$. For both experiments, CMS and ATLAS, emittance calculated from the measured $\Sigma$ in the crossing plane is significantly underestimated.

Therefore in these proceedings CMS emittance measurements only in noncrossing plane will be used for comparison to other instruments, based on the simple formula for emittance calculation:

$$\varepsilon_Y = \gamma\Sigma_Y^2/2\beta^* \tag{4}$$

## COMPARISON TO WIRE SCANNERS

### *Results from Fill 6592*

Fig. 5 shows the ratio of emittance measured in emittance scan 1 (green) and emittance scan 6 (black) to the WS emittance vs. the WS emittance. Emittance values per bunch crossing are listed in Table 1. Error bars on the WS emittance are estimated to be in the range of 4.6–4.9%, due to an uncertainty in $\beta^*$ of 2.0–2.5% at IP4 with all systematic sources included [6] and a 3% uncertainty in the WS beam width measurement. The uncertainty in the CMS emittance lies in the range of 3.6–4.6%, after propagating $\beta^*$ uncertainty of 3–3.6% and taking 2% uncertainty on the measured beam overlap to account for possible systematic bias due to fit model and beam-beam effects. The $\beta^*$ uncertainty at IP5 is derived based on the average of $\beta^*$ measurement using $k$-modulation for separate beams, as described in Ref. [7] and adding 2.0–2.5% in quadrature to statistical uncertainty to account for all possible sources of systematic uncertainty.

Emittance measured from CMS emittance scans is higher than WS emittance for all bunches. The difference is between 12 and 22%. The agreement between measurements from the

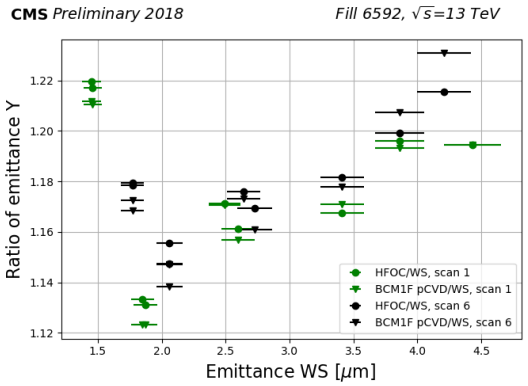


Figure 5: The ratio of emittance measured by CMS luminometers (HFOC shown with circles and BCM1F pCVD shown with triangles) to emittance measured by LHC WS in emittance scan 1 (green) and emittance scan 6 (black) in fill 6592 as a function of the WS emittance.

| BCID | $\varepsilon_Y^{\text{HFOC}}$ | | $\varepsilon_Y^{\text{BCM1F pCVD}}$ | | $\varepsilon_Y^{\text{WS}}$ | |
|---|---|---|---|---|---|---|
| | **sc. 1** | **sc. 6** | **sc. 1** | **sc. 6** | **sc. 1** | **sc. 6** |
| 4 | 5.29 | 5.12 | 5.29 | 5.18 | 4.43 | 4.21 |
| 451 | 4.62 | 4.63 | 4.61 | 4.66 | 3.86 | 3.86 |
| 1201 | 3.98 | 4.03 | 3.99 | 4.02 | 3.41 | 3.41 |
| 1501 | 2.92 | 3.10 | 2.91 | 3.10 | 2.29 | 2.64 |
| 1786 | 3.02 | 3.19 | 3.01 | 3.17 | 2.60 | 2.73 |
| 2101 | 2.12 | 2.38 | 2.10 | 2.37 | 1.87 | 2.06 |
| 2451 | 2.10 | 2.36 | 2.08 | 2.34 | 1.85 | 2.06 |
| 2801 | 1.77 | 2.09 | 1.76 | 2.08 | 1.45 | 1.77 |
| 3118 | 1.78 | 2.09 | 1.77 | 2.07 | 1.46 | 1.77 |

Table 1: Normalized emittance in $\mu$m measured by CMS luminometers (HFOC and BCM1F pCVD) and by LHC WS in emittance scan 1 ("sc. 1") and emittance scan 6 ("sc. 6") of the fill 6592 for nine colliding bunches.

two CMS luminometers is at the level of 1%. No beam-beam deflection or dynamic-$\beta^*$ corrections are applied, although the level of these corrections is not expected to exceed 1–2%. Work is ongoing at present to derive the correction based on a multiparticle approach [8, 9]. The relative change of emittance measured in scan 6 with respect to scan 1 by CMS and WS is shown in Fig. 6 in percent. A similar evolution is observed by both instruments: blow up of the narrow bunches and shrinkage of the wide bunches. For all bunches, except the one with the smallest emittance, CMS measures slightly lower or almost equal values of relative growth of emittance to WS.

Emittance ratios measured by CMS and WS are defined in Eqs. 5–6, where $\beta^*_{30,\text{IP5}}$ and $\beta^*_{25,\text{IP5}}$ ($\beta^*_{30,\text{IP4}}$ and $\beta^*_{25,\text{IP4}}$) correspond to $\beta^*$=30 and 25 cm at IP5 (IP4) at the time of emittance scans 1 and 6, respectively; $\Sigma_{1,\text{CMS}}$ and $\Sigma_{6,\text{CMS}}$ are the convoluted beam overlap widths, measured from CMS emittance scans 1 and 6; $\sigma_{1,\text{WS}}$ and $\sigma_{6,\text{WS}}$ are beam widths

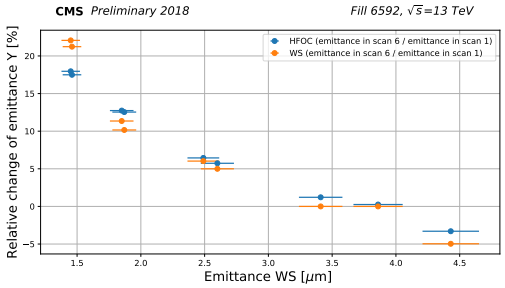


Figure 6: Relative growth of emittance in percent during fill 6592 comparing emittance scans 1 and 6, as measured by HFOC (blue) and WS (orange).

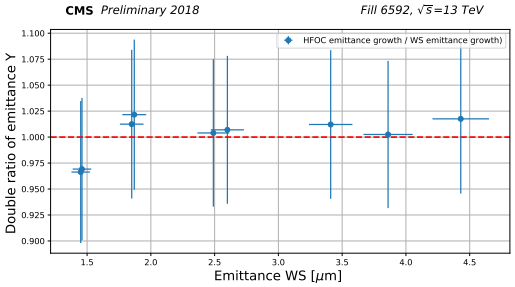


Figure 7: Double ratio of the relative growths of HFOC emittance, calculated using target $\beta^*$ value) to WS emittance.

measured by WS at IP4 at a time close to the corresponding CMS emittance scan.

$$R_{\varepsilon,\text{CMS}} = \frac{\varepsilon_{6,\text{CMS}}}{\varepsilon_{1,\text{CMS}}} = \frac{2\gamma\beta^*_{30,\text{IP5}}\Sigma^2_{6,\text{CMS}}}{2\gamma\beta^*_{25,\text{IP5}}\Sigma^2_{1,\text{CMS}}} \tag{5}$$

$$R_{\varepsilon,\text{WS}} = \frac{\varepsilon_{6,\text{WS}}}{\varepsilon_{1,\text{WS}}} = \frac{\gamma\beta^*_{30,\text{IP4}}\sigma^2_{6,\text{WS}}}{\gamma\beta^*_{25,\text{IP4}}\sigma^2_{1,\text{WS}}} \tag{6}$$

The double ratio of the emittance values is defined in Eq. 7 using the measured beam widths and target $\beta^*$=30 cm or 25 cm values. These double ratios are plotted per bunch crossing in Fig. 7.

$$\frac{R_{\varepsilon,\text{CMS}}}{R_{\varepsilon,\text{WS}}} = \frac{[\beta^*_{30,\text{IP5}}/\beta^*_{25,\text{IP5}}][\Sigma^2_{6,\text{CMS}}/\Sigma^2_{1,\text{CMS}}]}{[\beta^*_{30,\text{IP4}}/\beta^*_{25,\text{IP4}}][\sigma^2_{6,\text{WS}}/\sigma^2_{1,\text{WS}}]} \tag{7}$$

A similar ratio, but using measured $\beta^*$ with $k$-modulation instead of target $\beta^*$ value, is shown in Fig. 8. It is important to mention that for future operations it would be beneficial to add the measured $\beta^*$ during the beam commissioning at the IPs to the online publication to the experiments.

Assuming perfect measurement of $\beta^*$ at IPs and equal $\gamma$, deviation of the double ratio for the bunch with the lowest emittance from all other bunches points to a change of accuracy either of CMS emittance scans measurements or of WS at emittance values lower than 1.5 $\mu$m. Also the bias in the measured effective beam overlap by CMS in the case of non-Gaussian shape of narrow bunches should be evaluated.

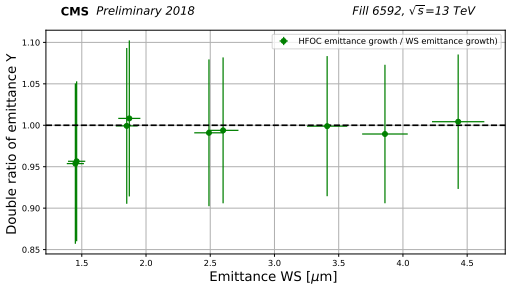


Figure 8: Double ratio of the relative growth of HFOC emittance to WS emittance. The $\beta^*$ used for the emittance calculation was measured with $k$-modulation for IP4 and IP5.

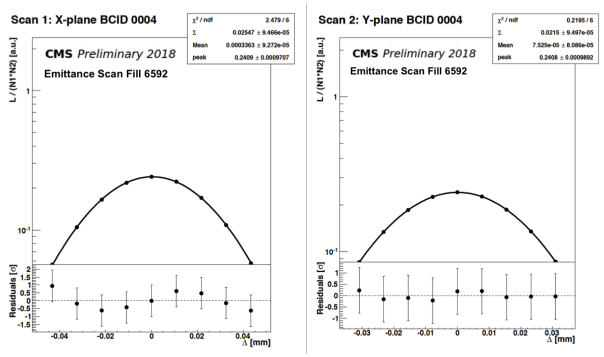


Figure 9: Normalized rate as a function of beam separation for a high-emittance bunch in the BSRT calibration fill 6592. Emittance scan in $X$ (left) and in $Y$ (right) are shown with a fit of a single Gaussian function.

Fig. 9 shows a fit to the normalized rate as a function of the beam separation of a single Gaussian function for a bunch with high emittance in $X$ and in $Y$ planes. The lower part of the plot shows the residuals. Slight "S-like" shape in the residuals of the scan in $X$ (left) is observed, but scan in $Y$ (right) is of good quality. It means that for wide bunches a single Gaussian fit is suitable and the 20% difference observed with respect to WS for this bunch (Fig. 5) is not related to the fit model.

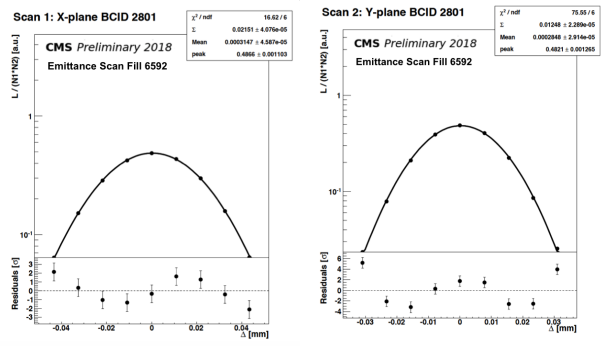


Figure 10: Normalized rate as a function of beam separation for a low-emittance bunch in the BSRT calibration fill 6592. Emittance scan in $X$ (left) and in $Y$ (right) are shown with a fit of a single Gaussian function.

Fig. 10 shows the same fits, but for the narrowest bunch. The S-like shape in the residuals of the scan in $X$ (left) is more pronounced, and a "W-like" shape is seen in the residuals in the $Y$ plane (right). Similar residual shapes were seen in ATLAS emittance scans, suggesting that this is a beam-related effect [10]. S-like shape in the residuals corresponds to the crossing plane of the experiment and W-like shape to the separation plane.

Fitting the rates measured in emittance scans in the $Y$ plane with a double Gaussian function resulted in maximum 1% effect on the measured effective beam overlap. The fraction of the second Gaussian in the fit did not exceed 3%, pointing to a Gaussian shape of the bunches in fill 6592. More about the effect of the fit function on the measured CMS beam overlap width is shown in the next section, based on the long scan of fill 7220, where low-emittance bunches were less Gaussian.

## *Results from Fill 7220*

There were several emittance scans and a long scan taken in fill 7220. The first emittance scan (hereafter referred to as emittance scan 1) was followed by the long scan (referred to as long scan 2). Here, we focus on the comparison of the results from emittance scan 1 and long scan 2 and study the effect of the different fit models on the measured $\Sigma_Y$.

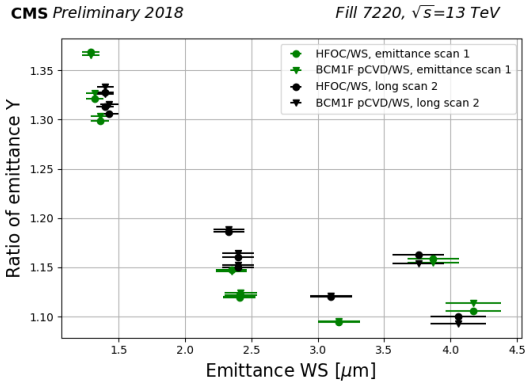


Figure 11: The ratio of emittance measured by CMS luminometers (HFOC shown by circles and BCM1F pCVD shown by triangles) to emittance measured by WS in emittance scan 1 (green) and long scan 2 (black) of the fill 7220.

Fig. 11 shows the ratio of emittance measured in emittance scan 1 (green) and long scan 2 (black) by CMS HFOC and BCM1F pCVD to emittance from WS. The emittance values measured by CMS for all bunches are higher than WS emittance. Differences between 9 and 20%, i.e., similar to the difference in fill 6592, are observed for most of the bunches, except for the first two bunches with emittance less than 1.5 $\mu$m.

The fraction of the non-Gaussian contribution for those bunches is estimated using double Gaussian (DG) and double Gaussian with a constant term (DGConst) fits for the long scan 2. As shown in Fig. 12, the fraction of the second Gaussian reaches maximum about 15%. This results in a

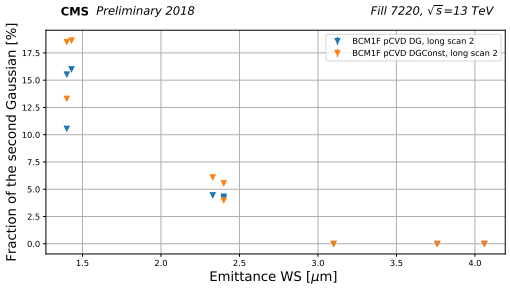


Figure 12: Fraction of the second Gaussian in the double Gaussian and double Gaussian with a constant term fits to the long scan 2 data, fill 7220.

maximum bias of 2.5% in the measured $\Sigma_Y$ when compared to $\Sigma_Y$ measured using a single Gaussian fits (SG). It partly explains the larger difference in the ratio of $\varepsilon_2^{\mathrm{CMS}}$ to $\varepsilon_2^{\mathrm{WS}}$, as shown in Fig. 11, but cannot explain the full difference of 15% for the low-emittance bunches relative to the other bunches. Example of a double Gaussian fit with constant term for the low-emittance bunch in long scan 2 is shown in Fig. 14. Flat residuals distribution at the bottom part of the plot proves that the fit describes the shape well.

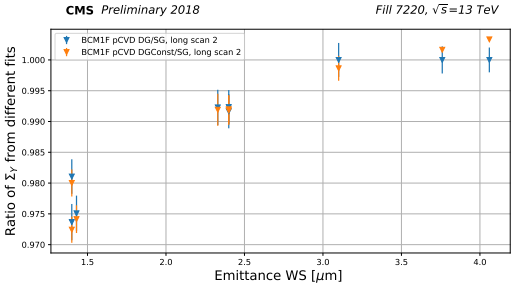


Figure 13: Ratio of $\Sigma_Y$ measured in long scan 2 using double Gaussian and double Gaussian with constant term fits to $\Sigma_Y$ measured using single Gaussian fits.

## EMITTANCE SCANS IN REGULAR LHC FILLS

In regular LHC fills about 2500 bunches are colliding at IP1/5. In long fills (10–12 hours), combining the results from emittance scans at the beginning of the fill and at the end of the fill, one can study the emittance evolution during the fill and compare it to the evolution measured by BSRT.

### *Corrections applied per bunch crossing*

Afterglow correction is applied per bunch crossing to correct for spillover of collisions from one bunch crossing to the following one and from material activation [3].

Also beam-beam correction should be taken into account per bunch crossing, as the level of the correction depends significantly on BCID, and the bunch intensity and widths are different at the beginning and at the end of the fill, therefore, affecting the level of the correction. An example of the

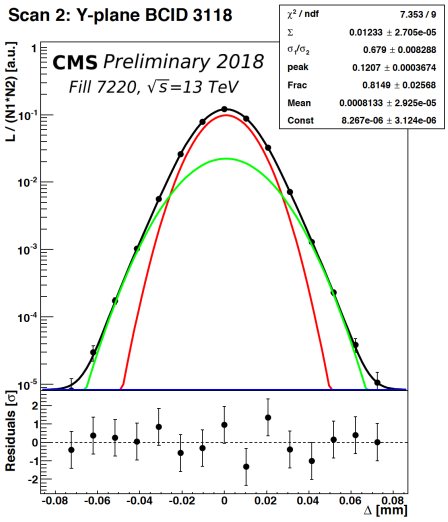


Figure 14: Normalized rate as a function of beam separation for the lowest emittance bunch in fill 7220. Double Gaussian with constant term fit and residuals distribution are shown.

beam-beam deflection corrections in the bunch trains, calculated using a single particle approach and Gaussian beam approximation [11], is shown in Fig. 15 for the emittance scan at the beginning of regular fill 7334. Work is ongoing to derive beam-beam correction based on a multiparticle approach and take into account emittance evolution during the fill [8, 9].

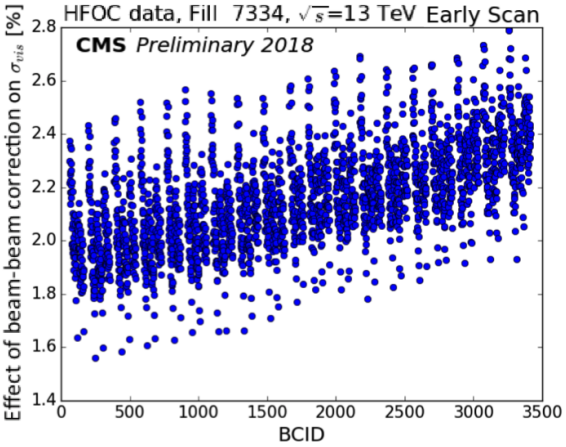


Figure 15: Beam-beam deflection correction in percent per bunch crossing on the visible cross-section, calculated based on a single particle approach and Gaussian beam approximation.

The normalization of the measurements provided by the Fast Bunch Current Transformers (FBCT) to the total current of the beam (DCCT) is done in every scan, and an additional correction of -1% to the FBCT current for the first bunch in the train is applied [12].

Due to the crossing angle and long range beam-beam interactions, the offset of the peak varies within the train

as shown in Fig. 16. To take into account this offset a peak position correction is derived assuming Gaussian shape of the beam and using the measured offset of the peak. The non-Gaussian shape of the bunch is the limitation of this method. If the offset is large and bunches have non-Gaussian shape, the peak correction has significant bias. To ensure centered positions of the beams before the scans, a beam optimization is required regularly before emittance scans in the future.

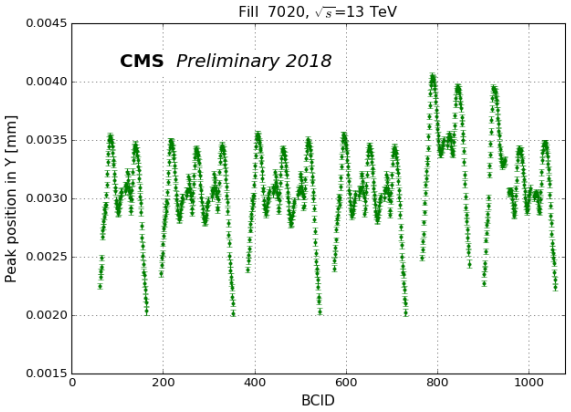


Figure 16: Position of the peak measured in the regular LHC fill 7020 in emittance scan $Y$. The repetitive pattern is due to long range beam-beam interactions in the bunch trains.

### *Effective beam overlap variation within a bunch train*

Beam evolution during collisions is caused by a combination of effects including burn-off, intrabeam scattering, beam-beam interactions, noise, as described in Ref. [13]. Emittance blow up, current losses and effect on the luminosity are also simulated and described in detail in Ref. [14].

The $\Sigma_X$ and $\Sigma_Y$ measured in the emittance scan at the end of the regular LHC fill 7334 is shown in Fig. 17 for all bunches (left) and zoomed into the first five bunch trains (right). Due to the crossing angle in $X$ plane, $\Sigma_X$ is larger than $\Sigma_Y$, but this is only a geometric effect. Beams are almost of equal size in $X$ and $Y$, about 14 $\mu$m. The first bunch in the train is wider than the rest of the bunches (machine effect, measured by all CMS luminometers).

To compensate for the bias in $\varepsilon_X$ at the beginning of the fill due to non-Gaussian longitudinal profile, an additional correction of +0.5 $\mu$m is applied. For the scan at the end of the fill, no additional correction is applied, as the beams are more Gaussian [4].

### *Emittance evolution during an LHC fill*

Similar to BSRT calibration fills, calculation of emittance from measured $\Sigma_{X(Y)}$ in emittance scans is done using Eq. 3-4. Fig. 18 and Fig. 19 show $\varepsilon_X$ and $\varepsilon_Y$ calculated based on HFOC $\Sigma_{X(Y)}$ measurements in the emittance scans at the beginning and an the end of fill 7334.

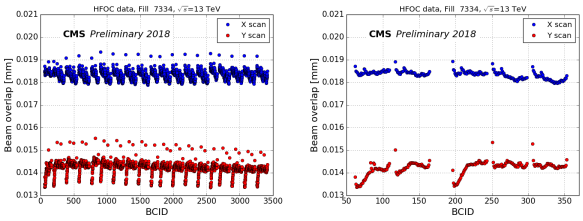


Figure 17: $\Sigma_X$ and $\Sigma_Y$ measured by HFOC in the emittance scan at the end of fill 7334. Left: all bunches, right: zoom into the first five bunch trains.

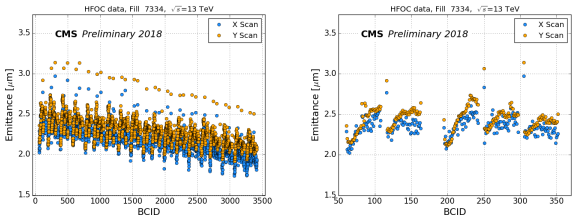


Figure 18: $\varepsilon_X$ and $\varepsilon_Y$ calculated using HFOC $\Sigma_{X(Y)}$ measurements in the emittance scan at the beginning of fill 7334. Left: all bunches, right: zoomed into the first five bunch trains.

Comparing panels on the left of the figures, where all bunches are shown, a slope arises in the emittance across the orbit at the beginning of the fill (Fig. 18), which becomes almost invisible by the end of the fill (Fig. 19). Comparing panels on the right of the figures, where only the first five bunch trains are shown, a slight change in $\varepsilon_Y$ and pronounced change in $\varepsilon_X$ along the trains are seen, in addition to the emittance growth towards the end of the fill in both planes.

## COMPARISON TO BSRT

Due to the potential bias from the longitudinal profiles [4] and crossing angle measurements [15] in the crossing plane emittance calculation ($\varepsilon_X$), we focus on $\varepsilon_Y$ comparison to BSRT measurements.

The difference between emittance at the end of the fill and at the beginning of the fill is considered as the measured emittance growth. Bunches show different evolution depending on the position in the train, and hence they were sub-divided into batches at the beginning and at the end

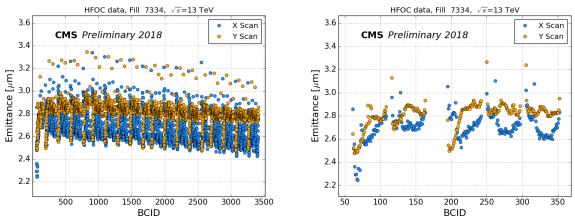


Figure 19: $\varepsilon_X$ and $\varepsilon_Y$ calculated using HFOC $\Sigma_{X(Y)}$ measurements in the emittance scan at the end of fill 7334. Left: all bunches, right: zoom into the first five bunch trains.

of the trains. For all batches in fill 7334, CMS measured about 10% less emittance growth than BSRT. However in fill 7221 (just after the BSRT calibration fill) CMS and BSRT measurements of the emittance growth agreed at the 2–3% level.

The $\varepsilon_Y$ measured from CMS emittance scans is consistently larger than BSRT $\varepsilon_Y$. The ratio between $\varepsilon_Y$ measured by CMS and BSRT varies in 10–25% range between fills and scans.

## CONCLUSIONS

Emittance scans at the experiments provide valuable measurement of emittance in the noncrossing plane. The bias on the measured effective beam overlap for non-Gaussian bunches is estimated to be up to 5% on the calculated $\varepsilon_Y$. However, most of the bunches in BSRT calibration fills are well described by single Gaussian fit. For Gaussian bunches, in CMS we measure 10–20% higher emittance than WS. Similar difference is observed when compared to BSRT, since BSRT is cross-calibrated to WS. Updated beam-beam corrections will be applied to emittance scans, and $\varepsilon_X$ calculation will be repeated using longitudinal profiles from CMS beam spot analyses.

In the future, longitudinal profile measurements are required close in time to emittance scans to improve $\varepsilon_X$ measurement from the experiments. Optimization scans before emittance scans should be included in the standard emittance scan procedure to avoid offsets. CMS and ATLAS emittance scans results are complementary and it will be beneficial to have emittance scans at the beginning and at the end of the long fills at both IPs to provide reference measurements in the noncrossing plane, and overall better understanding of the beam dynamics.

## ACKNOWLEDGMENT

The author would like to acknowledge colleagues from the CERN's Beams Department, in particular M. Hostettler, G. Trad, T. Argyropoulos, M. Hofer, and R. Tomas for multiple discussions, for providing WS data with the best corrections available, for discussions about the precision of different LHC measurements and for the offline longitudinal bunch profile analysis. Many thanks to the HSI working group, in particular I. Efthymiopoulos and S. Papadopoulou, for sharing their experience with the BSRT data analysis, including comparison of the BSRT measurements with the luminosity model. The author would like to acknowledge the large, ongoing effort from T. Pieloni and C. Tambasco from EPFL, to provide updated beam-beam corrections for emittance scans and thank them for fruitful discussions and collaboration.

## REFERENCES

[1] LHC Design Report - The LHC Main Ring, vol.1, CERN, 2004, DOI: 10.5170/CERN-2004-003-V-1

[2] G. Trad et al., Performance of the upgraded synchrotron radiation diagnostics at the LHC, Proceedings of the 7th International Particle Accelerator Conference, JAoW-IPAC2016-MOPMR030, https://cds.cern.ch/record/2207347

[3] CMS Collaboration, CMS luminosity measurement for the 2018 data-taking period at $\sqrt{s}$=13 TeV, CMS-PAS-LUM-18-002, https://cds.cern.ch/record/2676164

[4] M. Hostettler et al., Luminosity scans for beam diagnostics, Phys. Rev. Accel. Beams 21, (2018) 102801, DOI: 10.1103/PhysRevAccelBeams.21.102801

[5] O. Karacheban, P. Tsrunchev on behalf of the CMS Collaboration, Emittance scans for CMS luminosity calibration, EPJ Web of Conferences 201, 04001 (2019), DOI: 10.1051/epjconf/201920104001

[6] F. Carlier, R. Tomas, Accuracy and feasibility of the $\beta^*$ measurement for LHC and High Luminosity LHC using $k$ modulation, Phys. Rev. Accel. Beams 20, 011005 (2017), DOI: 10.1103/PhysRevAccelBeams.20.011005

[7] T. Persson et al., LHC optics correction in Run 2, 9th LHC Operations Evian Workshop, January 2019, https://indico.cern.ch/event/751857/contributions/3259376/

[8] T. Pieloni, Beam-beam simulations with COMBI and TRAIN in vdM fills, talk at LHC lumi days 2019, CERN, 5 June 2019, https://indico.cern.ch/event/813285/contributions/3406103

[9] V. Balagura, Simulation of beam-beam effects in vdM scans: impact on precision, talk at LHC lumi days 2019, CERN, 5 June 2019, https://indico.cern.ch/event/813285/contributions/3406102

[10] M. Hostettler et al., Observations from (OP) emittance scan analysis, talk at LHC Luminosity Calibration and Monitoring Working Group meeting, 23 July 2018, https://indico.cern.ch/event/745364/contributions/3080446

[11] A. Babaev on behalf of the CMS Collaboration, Beam-dynamic effects at the CMS BRIL van der Meer scans, CMS-CR-2017-415, https://cds.cern.ch/record/2304750

[12] J. Kral, Bunch-dependent response of FBCT with bunch trains, talk at LHC Luminosity Calibration and Monitoring Working Group meeting, 26 November 2018 https://indico.cern.ch/event/775187/contributions/3221928

[13] M. Lamont and O. Johnson, LHC beam and luminosity lifetimes revised, CERN-ACC-2014-0255, 2014

[14] F. Antoniou et al., Building a luminosity model for the LHC and HL-LHC, IPAC2015, Richmond, VA, USA, DOI: 10.18429/JACoW-IPAC2015-TUPTY020

[15] M. Hostettler et al., Impact of the crossing angle on luminosity asymmetries at the LHC in 2016 proton physics operation, Proceedings of IPAC2017, Copenhagen, Denmark, DOI: 10.18429/JACoW-IPAC2017-TUPVA005